Graphene-based mass sensors: Chaotic dynamics analysis using the nonlocal strain gradient model

Massoud Mir, Masoud Tahani*

Department of Mechanical Engineering, Ferdowsi University of Mashhad, Mashhad, Iran

A R T I C L E   I N F O

A B S T R A C T

Nonlinear oscillations of graphene resonators are unavoidable due to enhancing the mass sensitivity of graphene-based mass sensors and the nonlinear behavior of the systems provides the route to chaos. In this paper, the nonlinear and chaotic behavior of the graphene-based mass sensor is investigated. The nano-mechanical sensor includes an electrostatically actuated fully clamped single-graphene sheet as a nano-resonator with an attached concentrated mass. By neglecting the rotary inertia, the equation of motion of the nano-resonator and the attached mass is derived using the nonlocal strain gradient theory of elasticity. The nano-resonator is modeled as a Kirchhoff nano-plate with the von Kármán-type geometric nonlinearity. Applying the Galerkin decomposition method to the partial differential equation of motion leads to the ordinary differential equation. Based on the Melnikov's integral method two analytical criteria are derived which provide necessary conditions that determine the chaotic region of the system. The chaotic dynamics of the system are also scrutinized and verified through plotting the Lyapunov exponent diagram, phase plane trajectories and Poincaré maps.

1. Introduction

Nowadays, nanotechnology plays a significant role in our everyday life due to the outstanding properties of nano-structures and nanomaterials and much effort has been devoted to employ them in the synthesis of micro- and nano-scale systems. Micro-electromechanical systems (MEMS) and nano-electromechanical systems (NEMS) such as micro- and nano-scale switches, actuators and sensors are the main part of advances of nanotechnology that address the urgent issues in the modern industry.

Sensors play a vital role in many industrial and medical devices. Due to the pervasive demand for efficient and accurate sensors, many studies are underway on the design and development of more efficient sensors with different size and accuracy. Nano-scale sensors that have better performance, lower energy consumption and higher accuracy are called nanosensors.

A significant group of nano-sensors is mass nano-sensors that can be used to weigh small particles, bacteria and viruses. The main part of the mass nano-sensors is a nano-resonator that vibrates at its resonant frequency. One-dimensional resonators are a vibrating nano-beam, for example, a carbon nanotube and two-dimensional resonators containing a vibrating nano-plate, like a graphene sheet. The resonant frequency of the nano-resonator is changed when a tiny particle is attached

---

to it. By determining the shift in the resonance frequency of the new system, the tiny particle is weighted. Accurate mass nano-sensors have been designed and constructed which can weigh the particles that are around the mass of neutron and proton [1–3].

Since the discovery and introduction of graphene sheets in 2004 [4], this "miracle material" [5] has absorbed tremendous attention among the scientific and technological communities due to their superior electrical and mechanical properties and high-frequency which range up to the order of THz. The monolayer graphene sheet is a two-dimension crystal of covalently bonded carbon atoms with a theoretical thickness of 0.34 nm. Owing to exceptional properties of graphene, its applications even extend beyond that of the carbon nanotubes. Furthermore, graphene sheets can compensate for the defects of carbon nanotubes in geometry and orientation [6]. This unique characteristic has profound implications and has opened a new field which promises ultra-sensitive resonators. By following these features, Sakhaee-Pour et al. [7] proposed and investigated the potential applications of graphene sheets as a nano-resonator in miniature mass detectors. Hence, graphene becomes a potential candidate for fabricating graphene-based mass nano-sensors and motivate researchers to study on its vibrational properties.

Low-dimensional mechanical resonators are promising structures for nano-sensors. Considerable effort has been implemented for studying the dynamics of mechanical nano-resonators, such as carbon nanotubes and graphene. Li and Chou [8] predicted the fundamental frequencies of carbon nanotubes as nano-mechanical resonators using an atomistic modeling technique. They also investigated the effects of tube length, diameter and boundary conditions on the fundamental frequency of carbon nanotube resonator. Chen et al. [9] fabricated monolayer graphene resonator and study its response to changes in temperature and mass. They observed that the resonator show resonance in the megahertz range. Sadeghi and Naghdabadi [10] developed a hybrid atomistic–structural element for modeling the nonlinear behavior of graphene resonators. They also studied the effects of vibration amplitude and geometry of the graphene sheet on the fundamental frequency. Mianroodi et al. [11] used a membrane model to investigate the nonlinear vibration of single layer graphene sheet resonator. They concluded that by increasing the initial velocity and pretension, the nonlinear fundamental frequency of graphene resonator increased. Ouakad and Younis [12] used a two-dimensional nonlinear curved beam model to simulate the motions of a curved carbon nanotube resonator. They studied the influences of the level of slackness and the DC electrostatic load on the variation of natural frequencies and mode shapes of the resonator. Kang et al. [13] used molecular dynamics modeling and simulations to study the effect the tension variation on vibration of a tunable graphene-resonator which is suitable for use in nano-sensors. Eriksson et al. [14] used continuum elasticity theory to study circular nano-mechanical graphene resonators. They further obtained an analytic expressions for the eigen frequencies as functions of system parameters by solving the Airy stress problem. Lee et al. [15] exploited atomic finite element simulation to investigate the natural frequency and sensitivity of a graphene resonator with different boundary conditions utilizing the commercial code ANSYS. Their results show that the highest sensitivity is belong to fully clamped boundary condition of the graphene resonator. Caruntu and Luo [16] studied the nonlinear vibration of electrostatically actuated carbon nanotube resonator considering the damping and van der Waals forces. They utilized the multiple scales and reduced order model to investigate the damping, voltage and van der Waals effects on system behavior. Jiang et al. [17] utilized finite element modeling and simulation to study a pressure sensor with graphene nano-mechanical resonator. They calculated the resonance frequency of resonator as function of external pressure and found that the pressure sensitivity of the resonator can reach 26,838 Hz/kPa. Weber et al. [18] coupled multilayer graphene resonators to superconducting cavities to achieve a displacement sensitivity of 1.3 fm/ Hz$^{1/2}$. This low-dimensional resonator is a promising device for mass and force sensing experiments.

Various methods have been employed by researchers for modeling the mechanical properties of CNT and graphene such as molecular dynamics simulation, energy equivalent model, nonlocal theory of elasticity and nonlocal strain gradient theory of elasticity. Kang et al. [19] studied the vibrational properties of graphene resonator undergoing tensile loading via classical molecular dynamics simulations and estimated the resonance frequency versus tension. Shen et al. [20] utilized molecular dynamics simulation to investigate the effect of temperature on nonlinear vibration response of bilayer graphene sheets. Eltaher et al. [21] used an energy equivalent model to study the postbuckling stability of carbon nanotube surrounded by nonlinear elastic foundation. Wu et al. [22] utilized an energy-equivalent model to calculate the Young's modulus and shear modulus for both armchair and zigzag carbon nanotubes. Eltaher et al. [23] exploited an energy equivalent model to investigate the influence of the length scale parameter and orientation on the Young and shear moduli and the vibration behaviors of carbon nanotubes. Shen et al. [24] modeled a single layer graphene sheet as a nonlocal orthotropic plate to study its nonlinear vibration in thermal environment. The predicted results are remarkably near those are obtained from molecular dynamics simulations. Ansari et al. [25] analyzed the vibration of single-layered graphene sheets based on a nonlocal continuum plate model. They also exploit the molecular dynamics simulations to derive the appropriate values for the nonlocal parameter. Zhang et al. [26] studied the nonlinear vibration behavior of graphene sheets as a classical plate based on the nonlocal elasticity theory. They also examined the influences of aspect ratio, side length, boundary conditions and nonlocal parameters on the frequency–amplitude response of the system.

The nonlinear vibration of graphene sheets can be investigated on the basis of the non-classical theories of elasticity such as the nonlocal theory of elasticity and nonlocal strain gradient theory of elasticity. The impacts of both stress nonlocality and strain gradient size dependent effects are combined in the nonlocal strain gradient theory of elasticity. Hence, many studies have been conducted to utilize the non-classical theories of elasticity for nonlinear modeling of graphene sheets. Nematollahi et al. [27] analyzed the free vibration of graphene nano-plate based on the nonlocal strain gradient theory and classical plate theory. They studied the influence of temperature and small-scale parameters on the natural frequency of the

nano-plate. Ebrahimi and Barati [28] employed a nonlocal strain gradient plate model and investigated the effect of elastic foundation, temperature and nonlocal and length scale parameters on damping vibration of viscoelastic graphene sheets under hygro-thermal environments. Ebrahimi and Barati [29] also developed a nonlocal strain gradient model based on a two-variable shear deformation plate for vibration analysis of graphene sheets and studied the same parameters. Sahmani et al. [30] investigated the nonlinear response of functionally graded porous micro/nano-plates reinforced with graphene employing the nonlocal strain gradient theory. They displayed that for large amplitude vibrations the effect of porosity dispersion pattern on the nonlinear frequency becomes more important. Shahsavari et al. [31] presented a higher-order nonlocal strain-gradient model to analyze the damped vibration of the graphene sheet in the hygro-thermal environment. They studied the roles of small-scale parameters, viscous and damping coefficients, elastic foundation and hygrothermal environment on the vibrational responses of graphene sheets based on higher-order nonlocal strain gradient theory in conjunction with the Kirchhoff plate theory.

Due to the superb mechanical and vibrational properties of graphene, it can be used as a two dimensional resonator in mass nano-sensors. Sakhaee-Pour et al. [7] implemented molecular structural mechanics to study the vibrational behavior of graphene sheets. They calculated the fundamental frequencies of the graphene sheet with an attached mass to examine the possibility of using single-layered graphene sheets as mass sensors whose sensitivity is of the order of 10^{-6} fg (femtograms). Chen et al. [9] demonstrated the fabrication and electrical readout of the graphene sheet as a resonator and study its response due to the attached mass. Arash et al. [32] performed molecular dynamics simulations to study application of graphene sheets for the detection of gas atoms as mass sensors via the frequency shift of the system. They found that the resolution of a 10 nm square graphene sheet nano-resonator can achieve an order of 10^{-6} fg and the mass sensitivity is inversely proportional to the sizes of the graphene sheet. Jiang et al. [33] conducted molecular dynamics simulations to study the resonant frequency and mass sensitivity of graphene nano-resonators. They found that mass sensitivity can be enhanced simply by actuating nonlinear oscillations of graphene sheets instead of applying initial tensile strain to the resonators. Dai et al. [34] studied the nonlinear vibration of a graphene nano-resonator via the classical continuum elastic model. They found that the mass sensitivity of a graphene nano-resonator can be improved by inducing nonlinear vibration to it. Shen et al. [35] based on the nonlocal Kirchhoff plate theory studied the potential of the graphene sheet as a mass sensor. They found that the frequencies reduce to the results of the classical model by eliminating the nonlocal parameter. Their obtained results show that the increase in attached mass and approaching its position to the plate center, increase frequency shift and decreases the natural frequency. Lei et al. [6] examined the potential of a graphene-based mass sensor. They investigated the relationship between the attached nanoparticle and the frequency shift based on a continuum elastic model. Lee et al. [36] derived the frequency equation of the graphene with an attached mass based on nonlocal elasticity theory for simply supported rectangular graphene. Their results indicate that the frequency shift of the resonator increases when the nonlocal parameter is increased and the largest frequency shift and highest sensitivity are attained for the square geometrical resonator. Kwon et al. [37] employed molecular dynamics methods to estimate the shift in fundamental frequency of graphene nano-resonator with the attached mass. Murmu and Adhikari [38] derived a closed-form equation for the shift in frequency due to the added mass for rectangular graphene nano-resonators based on nonlocal elasticity. Wang and Arash [39] extensively reviewed the application of carbon nanotubes and graphene sheets as nano-resonator sensors for mass detection which provides an overview of the state of the art of recent research activities. Fazelzadeh and Ghavanloo [40] analyzed the vibration of the graphene sheet which can be employed in a mass nano-sensor. The frequency shift of the nano-sensor is also studied based on the nonlocal plate theory in thermal environment. Zhou et al. [41] explored the potential of the circular graphene sheet as a mass nano-sensor and employed nonlocal Kirchhoff plate theory to study vibrational behavior of the system. Jalali and Naei [42] employed molecular dynamics and nonlocal elasticity to investigate the application of graphene sheets as resonant sensors for the detection of nanoparticles. Karličić et al. [43] investigated the opportunity of graphene sheets to employ as a mass nano-sensor. They adopted the nonlocal Kirchhoff-Love plate theory to model graphene nano-resonator as an orthotropic nano-plate which is affected by the in-plane magnetic field. Jiang et al. [44] employed the nonlocal Kirchhoff plate theory to study the free vibration of a graphene sheet-based mass sensors and investigated the effect of some parameters on the frequency shift. Eltaher and Agwa [45] used an energy equivalent model to study the vibration characteristics of a pretension carbon nanotube resonator with an attached mass as a mass sensor. They found that carbon nanotube resonator can weigh a tiny mass of about $10-1$ zg. Ebrahimi and Barati [46] analyzed the vibration of graphene-based mass sensors resting on Winkler–Pasternak foundation under hygro-thermal environments via a two-variable shear deformation plate theory. They employed nonlocal strain gradient theory of elasticity to investigate the influence of length scale parameter, number of nanoparticles, nanoparticle mass and nonlocal parameter on vibrational behavior of the mass sensor.

Some studies have been devoted to study the nonlinear and chaotic behavior of graphene-based resonators due to the wide applications of them in the synthesis of precise mass nano-sensors. DeMartini et al. [47] predicted the chaotic behavior of micro-electromechanical oscillators which is governed by a version of the Mathieu equation. They performed numerical simulations to show that chaos can occur in this system and employed Melnikov's method to obtain an inequality for design purposes. Joshi et al. [48] studied the nonlinear vibration of doubly clamped wavy carbon nanotube-based mass sensor, wherein the carbon nanotube is excited harmonically near its primary resonance. They obtained fast Fourier transformation diagrams, Poincaré maps and time responses to analyze the dynamic behavior of the mass sensor. Joshi et al. [49] studied the nonlinear and chaotic vibration of carbon nanotube-based mass sensors. Their numerical investigations show that the

regions of chaotic and periodic behavior depend on the surface deviations and added mass. Jin et al. [50] investigated the chaotic synchronization of two coupled identical micro-resonators which is used for mass detection.

As previously mentioned, many studies have been focused on the nonlinear behavior of graphene sheets, which can be used as a two-dimensional nano-resonator in nano-sensors. Researchers have employed classical and non-classical theories of elasticity for modeling of nano-resonators. It is evident that the most comprehensive continuum theory for modeling the nano-structures is the nonlocal strain gradient theory of elasticity. These studies are mostly quantitative which lead to the solution of the equation of motion and determining the vibrational properties of nano-resonators. But very few of these studies have been devoted to qualitative behavior, namely, chaos prediction and nonlinear behavior investigation of NEMS. Since the resonance frequency of the nano-structures is on the order of kHz or MHz, the chaotic dynamics of these systems is potentially dangerous and the system may fail after a short time. Another important reason for examining the nonlinear behavior of graphene nano-resonators is that the nonlinear oscillations lead to enhancing the mass sensitivity of graphene-based mass sensors [33,34]. Therefore, the chaotic dynamics of the system must be predicted and controlled. In general, little research has been devoted to study the chaotic behavior of NEMS and MEMS, additionally, none of the attempts have employed nonlocal strain gradient theory for modeling the nano-systems. Finally, no research has been conducted so far on employing Melnikov's method to investigate the chaotic behavior of mass nano-sensors analytically.

This paper aims to study the qualitative behavior and chaotic dynamics of a graphene-based mass sensor. The sensor consists of a graphene-based nano-resonator with the attached mass under electrostatic excitation. The graphene nano-resonator is modeled as an isotropic Kirchhoff nano-plate with von Kármán-type non-linear strain-displacement relations in conjunction with nonlocal strain gradient theory of elasticity. Applying the Galerkin decomposition method to the equation of motion of the system, the obtained partial differential equation is reduced to the ordinary differential equation. Then the chaotic dynamics of mass nano-sensor is studied analytically employing the Melnikov's method which leads to an inequality as a parametric criterion that indicates the susceptible region of the system for chaos. Finally, abundant numerical simulations such as the largest Lyapunov exponent, phase plane trajectory and Poincaré map are also performed to verify the analytical results obtained from Melnikov's method.

2. Nonlocal strain gradient theory

Since the behavior of nano-scale materials is different from their major counterparts, researchers are motivated to develop the theory of elasticity for nano-scale modeling. Inspired by the works of Eringen [51,52] and Lam et al. [53], Lim et al. [54] combined the nonlocal theory of elasticity and the strain gradient theory of elasticity to introduce the nonlocal strain gradient theory of elasticity. Based on the nonlocal strain gradient theory [54], the strain energy (Π_U) of an isotropic elastic body can be written as

$$\Pi_U(\varepsilon_{ij}, \varepsilon'_{ij}, \alpha_0; \varepsilon_{ij,m}, \varepsilon'_{ij,m}, \alpha_1) = \frac{1}{2}\varepsilon_{ij}C_{ijkl}\int_V \alpha_0(|x-x'|, e_0a)\varepsilon'_{kl}dV'$$

$$+ \frac{l_m^2}{2}\varepsilon_{ij,m}C_{ijkl}\int_V \alpha_1(|x-x'|, e_1a)\varepsilon'_{kl,m}dV' \tag{1}$$

where ε_{ij} and ε'_{ij} are the strain tensor at point x and its neighbor points x' within domain V, respectively and C_{ijkl} is the tensor of elastic coefficients. $\alpha_0(|x-x'|, e_0a)$ and $\alpha_1(|x-x'|, e_1a)$ are attenuation kernel functions related to the nonlocal effect. e_0 and e_1 denote the nonlocal parameters to take into account the influence of stress nonlocality, a presents an internal characteristic length and l_m is the strain gradient length scale parameter.

Based on the nonlocal strain gradient theory of elasticity [54], the total stress of the nonlocal strain gradient theory can be defined as

$$t = \sigma - \nabla \cdot \sigma^{(1)} \tag{2}$$

where σ is the classical stress tensor and $\sigma^{(1)}$ is the higher-order stress tensor which correspond to the strain tensor ε and the strain gradient sensor $\nabla\varepsilon$, respectively. That is,

$$\sigma = \int_V \alpha_0(x', x, e_0a)C : \varepsilon'dV' \tag{3}$$

$$\sigma^{(1)} = l_m^2 \int_V \alpha_1(x', x, e_1a)C : \nabla\varepsilon'dV' \tag{4}$$

where ":" denotes the double-dot product.

To avoid employing an integral equation, Lim et al. [54] developed a general differential constitutive equation known as higher-order nonlocal strain gradient constitutive equation as

$$(1 - \mu_1\nabla^2)(1 - \mu_0\nabla^2)t_{ij} = C_{ijkl}(1 - \mu_1\nabla^2)\varepsilon_{kl} - C_{ijkl}\lambda(1 - \mu_0\nabla^2)\nabla^2\varepsilon_{kl} \tag{5}$$

where $\nabla^2 = \partial^2/\partial x^2 + \partial^2/\partial y^2$ is the Laplacian operator and for simplicity, it is considered that $(e_0a)^2 = \mu_0$, $(e_1a)^2 = \mu_1$ and $l_m^2 = \lambda$.

Assuming that $e_0 = e_1 = e$ or $\mu_0 = \mu_1 = \mu$, the general lower-order constitutive equation for nonlocal strain gradient is obtained as [54]

$$(1 - \mu \nabla^2)t_{ij} = C_{ijkl}(1 - \lambda \nabla^2)\varepsilon_{kl} \tag{6}$$

Let $\lambda=0$, Eq. (6) is transformed into constitutive equation of nonlocal elasticity theory [51,52] as follows:

$$(1 - \mu \nabla^2)t_{ij} = C_{ijkl}\varepsilon_{kl} \tag{7}$$

and letting $\mu=0$ in Eq. (6) leads to the constitutive equation of pure strain gradient elasticity theory of Aifantis [55] as follows:

$$t_{ij} = C_{ijkl}(1 - \lambda \nabla^2)\varepsilon_{kl} \tag{8}$$

In view of Eq. (6) the nonlocal strain gradient constitutive relation for an isotropic nano-plate can be expressed as

$$(1 - \mu \nabla^2)\begin{Bmatrix} t_{xx} \\ t_{yy} \\ t_{xy} \end{Bmatrix} = (1 - \lambda \nabla^2)\begin{bmatrix} Q_{11} & Q_{12} & 0 \\ Q_{12} & Q_{22} & 0 \\ 0 & 0 & Q_{66} \end{bmatrix}\begin{Bmatrix} \varepsilon_{xx} \\ \varepsilon_{yy} \\ \varepsilon_{xy} \end{Bmatrix} \tag{9}$$

where Q_{ij} are the plane-stress reduced stiffnesses

$$\begin{Bmatrix} Q_{11} \\ Q_{22} \\ Q_{12} \\ Q_{66} \end{Bmatrix} = \begin{Bmatrix} E/(1 - \nu^2) \\ E/(1 - \nu^2) \\ E\nu/(1 - \nu^2) \\ E/(1 + \nu) \end{Bmatrix} \tag{10}$$

where E is the Young's modulus and ν is the Poisson's ratio.

3. Governing dynamical equations

In this study, a fully clamped graphene sheet with an attached mass is considered for modeling of the two dimensional mass sensor (Fig. 1). It is assumed that the graphene sheet is a thin nano-plate and idealized as a classical Kirchhoff plate model. The components of displacement field for the graphene sheet within the basis of Kirchhoff plate theory can be expressed as

$$u_x(x, y, z, t) = -z\frac{\partial w(x, y, t)}{\partial x}$$
$$u_y(x, y, z, t) = -z\frac{\partial w(x, y, t)}{\partial y}$$
$$u_z(x, y, z, t) = w(x, y, t) \tag{11}$$

where $w(x, t)$ is the transverse displacement of any point on the mid-plane. The geometric nonlinearity imposed by large deflection of the graphene sheet is modeled based on the von Kármán theory. Therefore, the non-zero strains associated with the above displacement field (Eq. (11)) take the following form

$$\varepsilon_{xx} = \frac{1}{2}\left(\frac{\partial w}{\partial x}\right)^2 - z\frac{\partial^2 w}{\partial x^2}$$
$$\varepsilon_{yy} = \frac{1}{2}\left(\frac{\partial w}{\partial y}\right)^2 - z\frac{\partial^2 w}{\partial y^2}$$
$$\varepsilon_{xy} = \frac{1}{2}\left(\frac{\partial w}{\partial x}\right)\left(\frac{\partial w}{\partial y}\right) - z\frac{\partial^2 w}{\partial x \partial y} \tag{12}$$

The governing equation of motion of the graphene sheet and the attached mass can be derived using the extended Hamilton's principle

$$\int_{t_1}^{t_2} (\delta \Pi_U - \delta W_E - \delta K)dt = 0 \tag{13}$$

where $\delta \Pi_U$, δW_E and δK are the variation of strain energy, virtual work due to applied loads and virtual kinetic energy of the nano-sensor, respectively.

The details of the derivation of the equation of motion are presented in Appendix A. The final explicit expression of the governing equation of motion directly in terms of the displacement can be stated as follows:

$$\frac{\partial^2 w}{\partial x^2}\left\{(1 - \lambda \nabla^2)\left[A_{11}\left(\frac{\partial w}{\partial x}\right)^2 + A_{12}\left(\frac{\partial w}{\partial y}\right)^2\right]\right\}$$
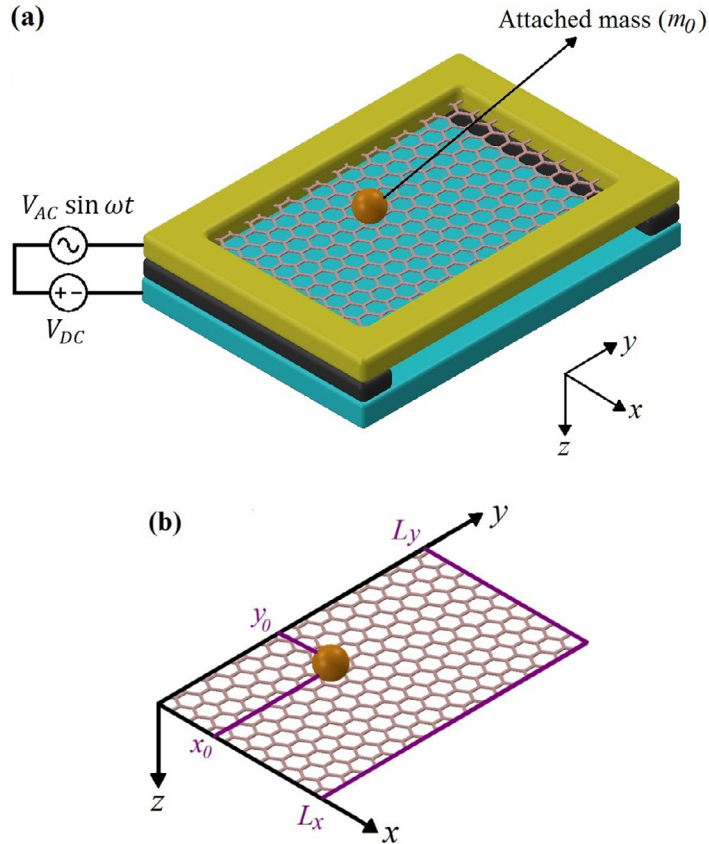
Fig. 1. Electrostatically actuated fully clamped graphene resonator with an attached mass.

$$+ 2A_{66} \frac{\partial^2 w}{\partial x \partial y} \left[(1 - \lambda \nabla^2) \left(\frac{\partial w}{\partial x} \frac{\partial w}{\partial y} \right) \right]$$

$$+ \frac{\partial^2 w}{\partial y^2} \left\{ (1 - \lambda \nabla^2) \left[A_{12} \left(\frac{\partial w}{\partial x} \right)^2 + A_{22} \left(\frac{\partial w}{\partial y} \right)^2 \right] \right\}$$

$$+ (1 - \lambda \nabla^2) \left[B_{11} \frac{\partial^4 w}{\partial x^4} + 2(B_{12} + B_{66}) \frac{\partial^4 w}{\partial x^2 \partial y^2} + B_{22} \frac{\partial^4 w}{\partial y^4} \right]$$

$$+ (1 - \mu \nabla^2) \left(F_E - C_D \frac{\partial w}{\partial t} \right)$$

$$= (1 - \mu \nabla^2) \left\{ [\rho h + m_0 \delta_D (x - x_0) \delta_D (y - y_0)] \frac{\partial^2 w}{\partial t^2} \right\} \tag{14}$$

In order to study the nonlinear dynamics of the graphene sheet and the attached mass regardless to its material properties and geometric characteristic, the following dimensionless quantities are introduced to normalize the equations of motion:

$$\bar{x} = \frac{x}{L_x}, \quad \bar{y} = \frac{y}{L_y}, \quad \bar{x}_0 = \frac{x_0}{L_x}, \quad \bar{y}_0 = \frac{y_0}{L_y}, \quad \bar{w} = \frac{w}{g}, \quad \bar{t} = \frac{h}{L_x L_y} \sqrt{\frac{E}{\rho}} t, \quad \bar{\omega} = \frac{L_x L_y}{h} \sqrt{\frac{\rho}{E}} \omega,$$

$$\bar{\mu} = \sqrt{\frac{\mu}{L_x L_y}}, \quad \bar{\lambda} = \sqrt{\frac{\lambda}{L_x L_y}}, \quad \bar{m} = \frac{1}{\rho h L_x L_y} m_0, \quad \bar{C}_D = \frac{L_x L_y}{h^2} \sqrt{\frac{1 - \nu^2}{\rho E}} C_D, \quad \bar{V} = \frac{V_{AC}}{V_{DC}},$$

$$\bar{\varepsilon} = \frac{L_x L_y (1 - \nu^2) V_{DC}^2 L^4}{2 E h^3 g^3} \varepsilon \tag{15}$$

It is noted that the Dirac delta function obeys the scaling property, in which $\delta_D(a^* x^*) = \delta_D(x^*)/a^*$ for $a^* > 0$. By employing the scaling property and substituting Eq. (33) into Eq. (32), the dimensionless form of the equation of motion can

be obtained as

$$
\begin{aligned}
&\frac{1}{L_x{}^2} \frac{\partial^2 \bar{w}}{\partial \bar{x}^2} \left\{ (1 - \bar{\lambda}^2 \bar{\nabla}^2) \left[\frac{A_{11}}{L_x{}^2} \left(\frac{\partial \bar{w}}{\partial \bar{x}} \right)^2 + \frac{A_{12}}{L_y{}^2} \left(\frac{\partial \bar{w}}{\partial \bar{y}} \right)^2 \right] \right\} \\
&+ \frac{2}{L_x{}^2 L_y{}^2} A_{66} \frac{\partial^2 \bar{w}}{\partial \bar{x} \partial \bar{y}} \left[(1 - \bar{\lambda}^2 \bar{\nabla}^2) \left(\frac{\partial \bar{w}}{\partial \bar{x}} \frac{\partial \bar{w}}{\partial \bar{y}} \right) \right] \\
&+ \frac{1}{L_y{}^2} \frac{\partial^2 \bar{w}}{\partial \bar{y}^2} \left\{ (1 - \bar{\lambda}^2 \bar{\nabla}^2) \left[\frac{A_{12}}{L_x{}^2} \left(\frac{\partial \bar{w}}{\partial \bar{x}} \right)^2 + \frac{A_{22}}{L_y{}^2} \left(\frac{\partial \bar{w}}{\partial \bar{y}} \right)^2 \right] \right\} \\
&+ \frac{1}{g^2} (1 - \bar{\lambda}^2 \bar{\nabla}^2) \left[\frac{B_{11}}{L_x{}^4} \frac{\partial^4 \bar{w}}{\partial \bar{x}^4} + \frac{2(B_{12} + B_{66})}{L_x{}^2 L_y{}^2} \frac{\partial^4 \bar{w}}{\partial \bar{x}^2 \partial \bar{y}^2} + \frac{B_{22}}{L_y{}^4} \frac{\partial^4 \bar{w}}{\partial \bar{y}^4} \right] \\
&+ \frac{Eh^3}{g^2 L_x{}^2 L_y{}^2} (1 - \bar{\mu}^2 \bar{\nabla}^2) \left(\bar{\varepsilon} \bar{F}_E - \bar{C}_D \frac{\partial \bar{w}}{\partial \bar{t}} \right) \\
&= \frac{Eh^3}{g^2 L_x{}^2 L_y{}^2} (1 - \bar{\mu}^2 \bar{\nabla}^2) \left\{ [1 + \bar{m} \delta_D(\bar{x} - \bar{x}_0) \delta_D(\bar{y} - \bar{y}_0)] \frac{\partial^2 \bar{w}}{\partial \bar{t}^2} \right\}
\end{aligned}
\tag{16}
$$

in which $\bar{F}_E$ is as follows:

$$
\bar{F}_E = \frac{(1 + \bar{V} \sin \bar{\omega} \bar{t})^2}{(1 - \bar{w})^2}
\tag{17}
$$

and $\bar{\nabla}^2$ is defined as

$$
\bar{\nabla}^2 = \frac{L_y}{L_x} \frac{\partial^2}{\partial \bar{x}^2} + \frac{L_x}{L_y} \frac{\partial^2}{\partial \bar{y}^2}
\tag{18}
$$

Due to the small magnitude of AC voltage compared to the DC voltage [56–59], which leads to the small value of $\bar{V} = V_{AC}/V_{DC}$, Eq. (17) can be reduced to

$$
\bar{F}_E = \frac{1 + 2\bar{V} \sin \bar{\omega} \bar{t}}{(1 - \bar{w})^2}
\tag{19}
$$

Nonlinear term of Eq. (17) can be approximated through Taylor's series expansion. Employing a fifth-order Taylor's series expansion with respect to $\bar{w}$, the dimensionless electrostatic force $\bar{F}_E$ is obtained as

$$
\bar{F}_E = (1 + 2\bar{w} + 3\bar{w}^2 + 4\bar{w}^3 + 5\bar{w}^4 + 6\bar{w}^5)(1 + 2\bar{V} \sin \bar{\omega} \bar{t})
\tag{20}
$$

Since the first-mode analysis of electrically actuated micro/nano-plates may be accurate [38,60,61], the dimensionless deflection of the rectangular micro/nano-plate based on the one-mode solution is expressed as

$$
\bar{w}(\bar{x}, \bar{y}, \bar{t}) = \nu(\bar{x}, \bar{y}) . \phi(\bar{t})
\tag{21}
$$

where $\nu(\bar{x}, \bar{y})$ is the normalized eigenfunction that satisfies the boundary conditions of the fully clamped nano-resonator and $\phi(\bar{t})$ is the generalized time coordinate. Here, $\nu(\bar{x}, \bar{y})$ for a fully clamped nano-plate is as follows [62]:

$$
\nu(\bar{x}, \bar{y}) = (\cos 2\pi \bar{x} - 1)(\cos 2\pi \bar{y} - 1)
\tag{22}
$$

According to the Galerkin method, by substituting Eq. (21) into Eq. (16), then multiplying the obtained equation by $\nu(\bar{x}, \bar{y})$ and integrating with respect to both $\bar{x}$ and $\bar{y}$ over the interval [0,1], one can obtain the following nonlinear ordinary differential equation

$$
\begin{aligned}
&\ddot{\phi} + \alpha \dot{\phi} + \beta_0 + \beta_1 \phi + \beta_2 \phi^2 + \beta_3 \phi^3 + \beta_4 \phi^4 + \beta_5 \phi^5 \\
&= (c_0 + c_1 \phi + c_2 \phi^2 + c_3 \phi^3 + c_4 \phi^4 + c_5 \phi^5) \sin \bar{\omega} \bar{t}
\end{aligned}
\tag{23}
$$

in which the coefficients α, β_i and c_i ($i = 0, 1, 2$ and 5) are given in Appendix A and a dot over a function in Eq. (23) denotes differentiation with respect to $\bar{t}$.

4. Chaotic behavior analysis

4.1. Homoclinic and heteroclinic bifurcations

In order to investigate the chaotic behavior of mass nano-sensor, the first step is to rewrite Eq. (23) in the state space by defining the auxiliary variable ψ as

$$\dot{\phi} = \psi$$
$$\dot{\psi} = -\alpha\psi - \beta_0 - \beta_1\phi - \beta_2\phi^2 - \beta_3\phi^3 - \beta_4\phi^4 - \beta_5\phi^5$$
$$+ (c_0 + c_1\phi + c_2\phi^2 + c_3\phi^3 + c_4\phi^4 + c_5\phi^5)\sin(\bar{\omega}\bar{t}) \tag{24}$$

Assuming that the second relation of Eq. (24) can be divided into two perturbed and unperturbed counterparts as follows:

$$\dot{\phi} = \psi$$
$$\dot{\psi} = -\beta_0 - \beta_1\phi - \beta_2\phi^2 - \beta_3\phi^3 - \beta_4\phi^4 - \beta_5\phi^5$$
$$+ \varepsilon\left[-\alpha\psi + (c_0 + c_1\phi + c_2\phi^2 + c_3\phi^3 + c_4\phi^4 + c_5\phi^5)\sin\bar{\omega}\bar{t}\right] \tag{25}$$

hence, the unperturbed system can be separated as follows:

$$\dot{\phi} = \psi$$
$$\dot{\psi} = -\beta_0 - \beta_1\phi - \beta_2\phi^2 - \beta_3\phi^3 - \beta_4\phi^4 - \beta_5\phi^5 \tag{26}$$

The Hamiltonian of the unperturbed system (Eq. (26)) which represents the total energy of the system is also obtained as

$$H(\phi, \psi) = U(\phi) + \frac{1}{2}\psi^2 \tag{27}$$

where $U(\phi)$ is the associated potential function of this Hamiltonian system:

$$U(\phi) = \beta_0\phi + \frac{1}{2}\beta_1\phi^2 + \frac{1}{3}\beta_2\phi^3 + \frac{1}{4}\beta_3\phi^4 + \frac{1}{5}\beta_4\phi^5 + \frac{1}{6}\beta_5\phi^6 \tag{28}$$

The first derivative of $U(\phi)$ with respect to ϕ is of the following form

$$\frac{dU(\phi)}{d\phi} = \beta_0 + \beta_1\phi + \beta_2\phi^2 + \beta_3\phi^3 + \beta_4\phi^4 + \beta_5\phi^5 \tag{29}$$

Equating the right-hand of Eq. (29) to zero, leads to a quintic function which is proved in mathematics that has at most five real roots. These roots are the extremums of the potential function (Eq. (28)). In this work, the comprehensive case with five extremums will be studied. A simple case (with $\beta_0 = \beta_2 = \beta_4 = \beta_5 = 0$) is thoroughly studied in the literature (e.g. [57,63]).

Figs. 2(a) and 3(a) show the Hamiltonian function (Eq. (27)) and the potential energy (thick black line) for two sets of given values of β_i ($i = 0, 1, 2, ... 5$). Fig. 2(a) shows a double-well and triple-hill potential function and Fig. 3(a) shows a triple-well and double-hill potential function. Figs. 2(b) and 3(b) show the corresponding phase space contour plot for Figs. 2(a) and 3(a), respectively. It can be inferred from Figs. 2(b) and 3(b) that the dynamical system of mass nano-sensor is prone to the occurrence of homoclinic or heteroclinic bifurcations depending to the sign of parameters β_i ($i = 0, 1, 2, ... 5$). Homoclinic and heteroclinic bifurcations are indicative of the chaotic behavior of the system whose stable and unstable manifolds intersect transversally.

4.2. Homoclinic and heteroclinic orbits

Homoclinic and heteroclinic orbits of the mass nano-sensor can be determined by solving Eq. (27) along with the fact that these orbits pass through the saddle point:

$$\dot{\phi} = \pm\sqrt{2\left[H_{Saddle} - \left(\beta_0\phi + \frac{1}{2}\beta_1\phi^2 + \frac{1}{3}\beta_2\phi^3 + \frac{1}{4}\beta_3\phi^4 + \frac{1}{5}\beta_4\phi^5 + \frac{1}{6}\beta_5\phi^6\right)\right]} \tag{30}$$

where H_{Saddle} is the value of the Hamiltonian at its saddle point.

Solving the obtained differential equation (Eq. (30)) presents a great challenge which may lead to a complicated equation which makes it impossible to solve the Melnikov's integral. Therefore, the homoclinic and heteroclinic orbits of the well-known Duffing equation are employed to approximate the homoclinic and heteroclinic orbits of the system, respectively [56,58,64]. A most general form of the Duffing equation is

$$\ddot{\phi} + \alpha\dot{\phi} + \beta_1\phi + \beta_3\phi^3 = F_D\cos\omega_D t \tag{31}$$

the homoclinic orbit of the Duffing equation can be obtained by solving Eq. (30) with $\beta_0 = \beta_2 = \beta_4 = \beta_5 = 0$ as follows:

$$\Gamma_{Hom}(\bar{t}) : \left(\phi_{Hom}(\bar{t}), \psi_{Hom}(\bar{t})\right) \tag{32}$$

where
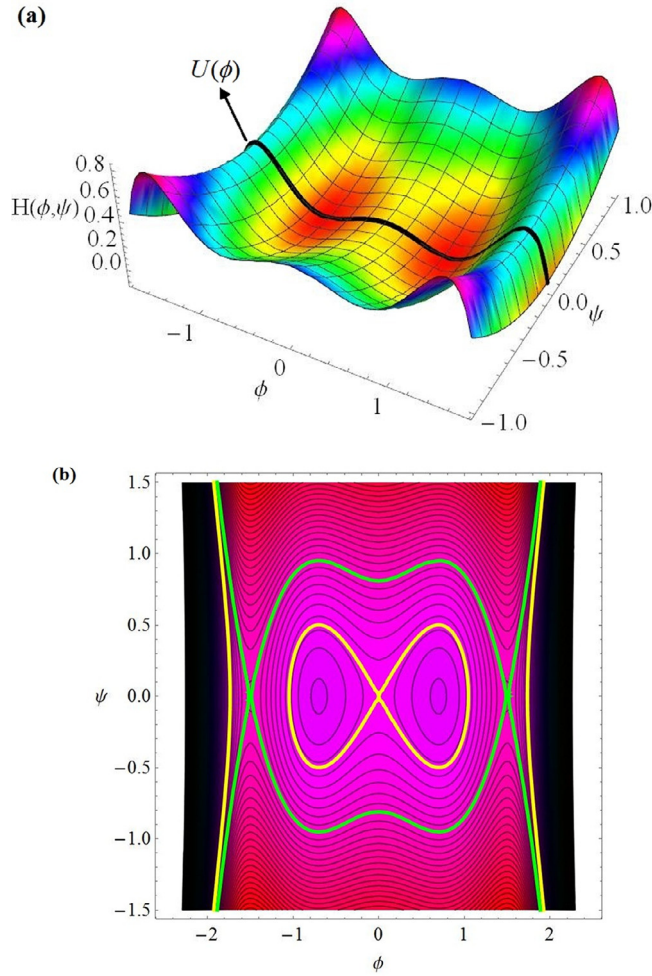
Fig. 2. (a) Sketch of the Hamiltonian surface $H(\phi,\psi)$ and the potential curve $U(\phi)$; (b) the corresponding phase space contour plot. The parameters are set as $\beta_0 = \beta_2 = \beta_4 = 0$, $\beta_1 = -1.1025$, $\beta_3 = 2.74$, $\beta_5 = -1$.

$$\phi_{Hom}(\bar{t}) = \sqrt{\frac{-2\beta_1}{\beta_3}} sech\left(\sqrt{-\beta_1}\bar{t}\right)$$
$$\psi_{Hom}(\bar{t}) = \beta_1 \sqrt{\frac{2}{\beta_3}} sech\left(\sqrt{-\beta_1}\bar{t}\right) \tanh\left(\sqrt{-\beta_1}\bar{t}\right)$$
(33)

and the heteroclinic orbit of the Duffing equation can be determined as

$$\Gamma_{Het}(\bar{t}) : \left(\phi_{Het}(\bar{t}), \psi_{Het}(\bar{t})\right)$$
(34)

where

$$\phi_{Het}(\bar{t}) = \sqrt{\frac{-\beta_1}{\beta_3}} \tanh\left(\sqrt{\frac{\beta_1}{2}}\bar{t}\right)$$
$$\psi_{Het}(\bar{t}) = \frac{\beta_1}{\sqrt{-2\beta_3}} sech^2\left(\sqrt{\frac{\beta_1}{2}}\bar{t}\right)$$
(35)

It is worth mentioning that the existence of two different solutions for Eq. (30) is because of the different values of H_{Saddle} for homoclinic and heteroclinic phenomena.
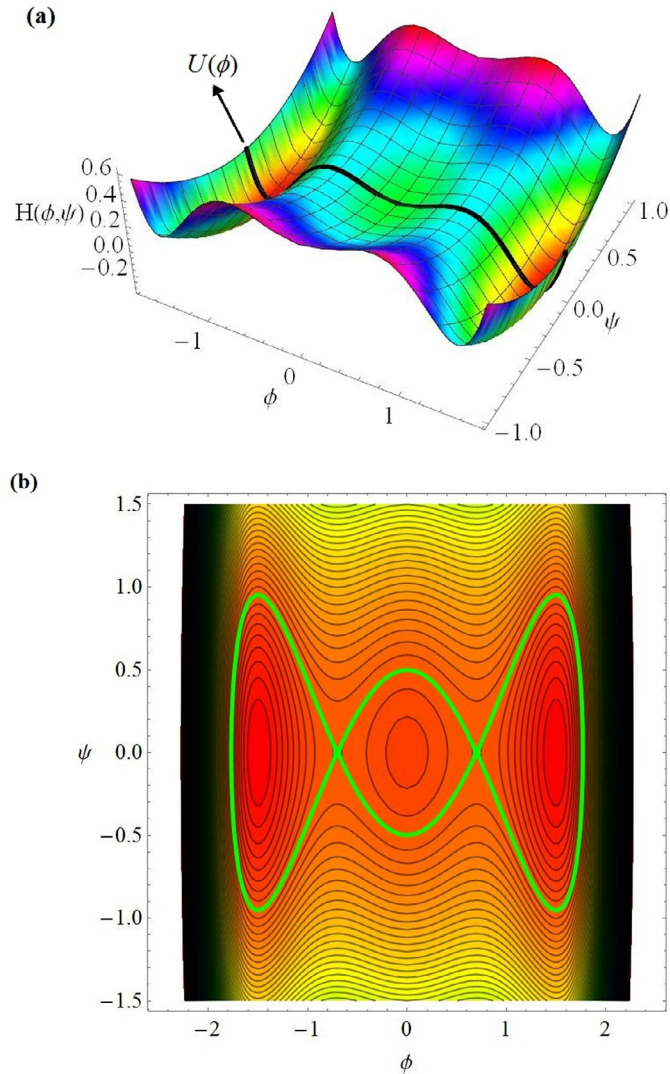
Fig. 3. (a) Sketch of the Hamiltonian surface $H(\phi,\psi)$ and potential curve $U(\phi)$; (b) the corresponding phase space contour plot. The parameters are set as $\beta_0= \beta_2= \beta_4=0$, $\beta_1=1.1025$, $\beta_3=-2.74$, $\beta_5=1$.

4.3. Melnikov analysis

Melnikov's integral method will be employed in this section for analyzing the chaotic nature of graphene-based mass sensors. Homoclinic and heteroclinic bifurcations are global bifurcations that often occur due to the transverse intersection of perturbed stable and unstable manifolds and can be accompanied by the onset of transition to chaos. Melnikov's integral method provides an analytical rule as a criterion for the transition to chaos by determining the distance between the stable and unstable manifolds of the perturbed system [65–67]. In this work, two Melnikov analysis are implemented on the nano-resonator equation Eq. (25)) distinctly employing the homoclinic and heteroclinic orbits of the Duffing oscillator (Eqs. (32) and ((34), respectively).

Considering the state space equation of the perturbed system (Eq. (25)) and employing the equations of homoclinic or heteroclinic orbits, the Melnikov function is expressed as [65–67]

$$
\begin{aligned}
M(\bar{t}_0) = & \int_{-\infty}^{+\infty} -\alpha \psi(\bar{t})^2 d\bar{t} \\
& + \int_{-\infty}^{+\infty} \psi(\bar{t})\Big(c_0 + c_1\phi(\bar{t}) + c_2\phi(\bar{t})^2 + c_3\phi(\bar{t})^3 + c_4\phi(\bar{t})^4 + c_5\phi(\bar{t})^5\Big) \sin\bar{\omega}(\bar{t} - \bar{t}_0)d\bar{t}
\end{aligned}
\tag{36}
$$

in which t_0 is the cross-section time of the Poincaré map [68].

The Melnikov function of homoclinic orbit can be determined by letting $\phi = \phi_{Hom}$ and $\psi = \psi_{Hom}$ and substituting the homoclinic orbit from Eq. (33) into Eq. (36) as follows:

$$
120\alpha\beta_1{}^2\beta_3 + \frac{\pi\omega}{\sqrt{-\beta_3}}\Bigg[\sqrt{\frac{-\beta_1}{\beta_3}}\,\omega[15\beta_3\left(-4c_3\beta_1 + 6c_1\beta_3 + c_3\omega^2\right)
$$

$$
+ c_5(64\beta_1{}^2 - 20\beta_1\omega^2 + \omega^4)]csc\left(\frac{\pi\omega}{2\sqrt{\beta_1}}\right) + 3\sqrt{2\beta_1}[10\beta_3\left(-c_2\beta_1 + 3c_0\beta_3 + c_2\omega^2\right)
$$

$$
+ c_4(9\beta_1{}^2 - 10\beta_1\omega^2 + \omega^4)]\sec\left(\frac{\pi\omega}{2\sqrt{\beta_1}}\right)\Bigg]\cos\left(\omega\bar{t}_0\right) = 0 \tag{37}
$$

The following criterion can be obtained as a necessary but not sufficient condition for the homoclinic chaos in graphene-based mass sensor

$$
\left|\left[120\alpha\beta_1{}^2\beta_3\right]\Bigg/\left\{\frac{\pi\omega}{\sqrt{-\beta_3}}\Bigg[\sqrt{\frac{-\beta_1}{\beta_3}}\,\omega\left[15\beta_3(-4c_3\beta_1 + 6c_1\beta_3 + c_3\omega^2)\right.\right.\right.
$$

$$
+ c_5(64\beta_1{}^2 - 20\beta_1\omega^2 + \omega^4)\Big]csc\left(\frac{\pi\omega}{2\sqrt{\beta_1}}\right) + 3\sqrt{2\beta_1}\left[10\beta_3(-c_2\beta_1 + 3c_0\beta_3 + c_2\omega^2)\right.
$$

$$
\left.\left.\left.+ c_4(9\beta_1{}^2 - 10\beta_1\omega^2 + \omega^4)\right]\sec\left(\frac{\pi\omega}{2\sqrt{\beta_1}}\right)\right\}\right| \leq 1 \tag{38}
$$

Similarly, letting $\phi = \phi_{Het}$ and $\psi = \psi_{Het}$ and after substitution of the heteroclinic orbit from Eq. (35) into Eq. (36), the Melnikov function of heteroclinic orbit can be obtained as

$$
\frac{60\alpha\beta_1{}^2\beta_3\sqrt{-2\beta_3}}{\pi\omega}\sinh\left(\frac{\pi\omega}{\sqrt{2\beta_1}}\right)
$$

$$
+ \omega\sqrt{\frac{-\beta_1}{\beta_3}}[15\beta_3\left(-4c_3\beta_1 + 6c_1\beta_3 + c_3\omega^2\right) + c_5(46\beta_1{}^2 - 20\beta_1\omega^2 + \omega^4)]\cos\left(\omega\bar{t}_0\right)
$$

$$
+ 3\sqrt{2\beta_1}[10\beta_3\left(-c_2\beta_1 + 3c_0\beta_3 + c_2\omega^2\right) + c_4(6\beta_1{}^2 - 10\beta_1\omega^2 + \omega^4)]\sin\left(\omega\bar{t}_0\right) = 0 \tag{39}
$$

The trigonometric R method can be employed to find an inequality as a criterion. Therefore, the following criterion is determined as a necessary condition for the heteroclinic chaos in graphene-based mass sensor

$$
\left|\left[\frac{60\alpha\beta_1{}^2\beta_3\sqrt{-2\beta_3}}{\pi\omega}\sinh\left(\frac{\pi\omega}{\sqrt{2\beta_1}}\right)\right]^2\Bigg/\left\{\left[\omega\sqrt{\frac{-\beta_1}{\beta_3}}\left(\begin{array}{c}15\beta_3(-4c_3\beta_1 + 6c_1\beta_3 + c_3\omega^2)\\ +c_5(46\beta_1{}^2 - 20\beta_1\omega^2 + \omega^4)\end{array}\right)\right]^2\right.\right.
$$

$$
\left.\left.+ \left[3\sqrt{2\beta_1}\left(10\beta_3(-c_2\beta_1 + 3c_0\beta_3 + c_2\omega^2) + c_4(6\beta_1{}^2 - 10\beta_1\omega^2 + \omega^4)\right)\right]^2\right\}\right| \leq 1 \tag{40}
$$

5. Numerical simulations

Chaotic dynamics of the graphene-based mass sensor was studied analytically in the previous section. In this section, some numerical verifications are performed to illustrate the chaotic behavior of the graphene-based mass sensor. To do so, the Lyapunov exponent diagram, phase plane trajectory and the Poincaré map will be obtained based on Eq. (24).

The Lyapunov exponent is a typical indicator for chaos detection which can be calculated based on the algorithm which is proposed in Ref. [69]. A positive Lyapunov exponent indicates the sensitivity of the system to the initial conditions which is leading to the formation of a strange attractor in the system's state space and signifies the chaotic behavior of the system. The Lyapunov exponents of the variables ϕ and ψ for the given value of parameters are plotted in Figs. 4 and 5. The positive Lyapunov exponents imply the chaotic behavior of the graphene-based mass sensor.

Phase plane trajectories of the system for the given value of parameters are depicted in Figs. 6 and 7, which qualitatively demonstrate the existence of chaos in the behavior of the graphene-based mass sensor.

The Poincaré maps of the system are illustrated in Figs. 8 and 9 for the same values of parameters as given in Figs. 6 and 7, respectively. Scattered points appearing within the Poincaré maps, qualitatively confirmed the chaotic nature of the graphene-based mass sensor.

Phase plane trajectories and Poincaré maps intuitively show the dynamics of the system and their complexity are indicative of the chaotic behavior of the system. These figures are very simple for regular and periodic systems. For example, the phase plane trajectories and Poincaré maps of a periodic motion will be an ellipse and a point, respectively.
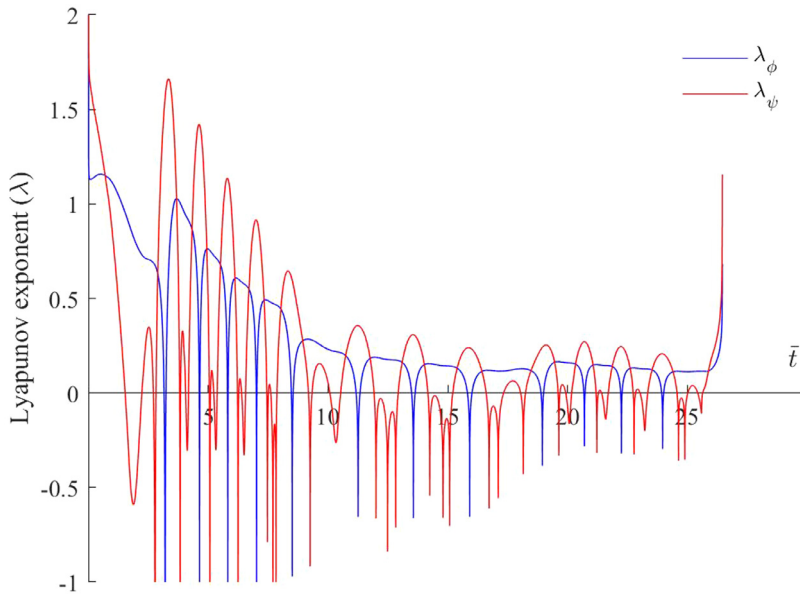
Fig. 4. The Lyapunov exponents of the system. The parameters are set as $\beta_0=-0.14112$, $\beta_1=-0.6888$, $\beta_2=0.508$, $\beta_3=2.14$, $\beta_4=-0.1$, $\beta_5=0.23$, $\alpha=0.05$, $\omega=0.8$, $c_0=0.1$, $c_1=0.2$, $c_2=0.3$, $c_3=0.4$, $c_4=0.5$ and $c_5=0.6$ with initial conditions: $\phi(0)=0.1$ and $\psi(0)=0.25$.
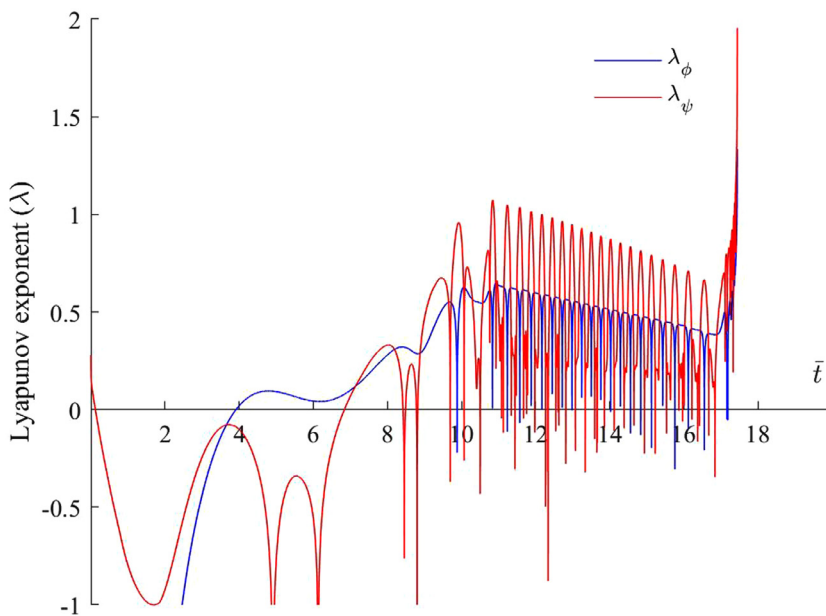
Fig. 5. The Lyapunov exponents of the system. The parameters are set as $\beta_0=0.14112$, $\beta_1=0.6888$, $\beta_2=-0.508$, $\beta_3=-2.14$, $\beta_4=0.1$, $\beta_5=0.59$, $\alpha=0.05$, $\omega=0.8$, $c_0=0.1$, $c_1=0.2$, $c_2=0.3$, $c_3=0.4$, $c_4=0.5$ and $c_5=0.6$ with initial conditions: $\phi(0)=0.1$ and $\psi(0)=0.25$.

6. Results and discussions

A graphene-based mass sensor is comprised of a graphene sheet as a resonator with an attached mass which vibrates at its resonant frequency. In this study, a fully clamped graphene sheet is considered for modeling the two-dimensional nano-resonator. Practically, this boundary condition is closer to the actual conditions of the nano-sensor and is easier to construct. The sensitivity of resonator with fully clamped boundary condition is the highest in comparison with the other boundary conditions [15]. For the other boundary conditions, only Eq. (22) should be replaced with relevant eigenfunction and the rest of the steps of the procedure are the same as this study.
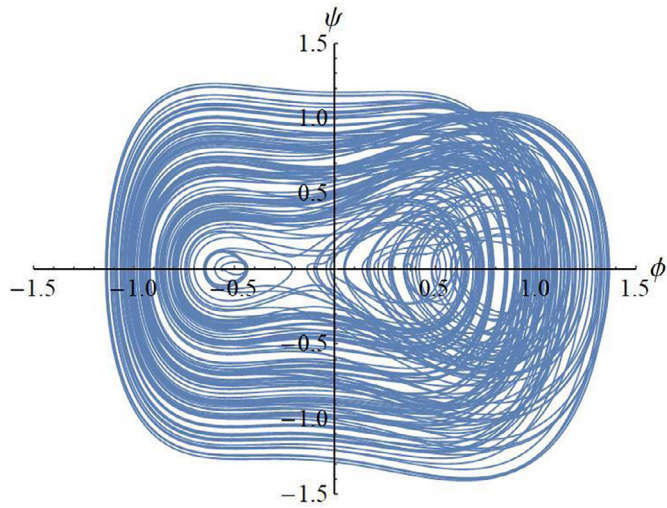
Fig. 6. Phase plane trajectories of the system for $\beta_5=0.8$ and the other parameter values as in Fig. 4.
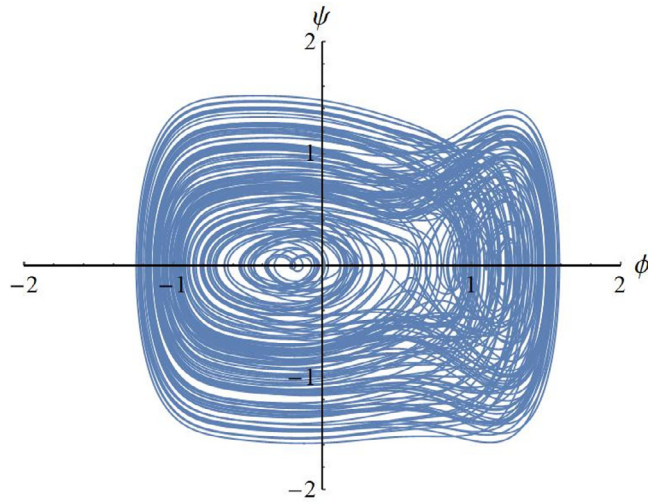
Fig. 7. Phase plane trajectories of the system for $\beta_5=2.7$ and the other parameter values as in Fig. 5.
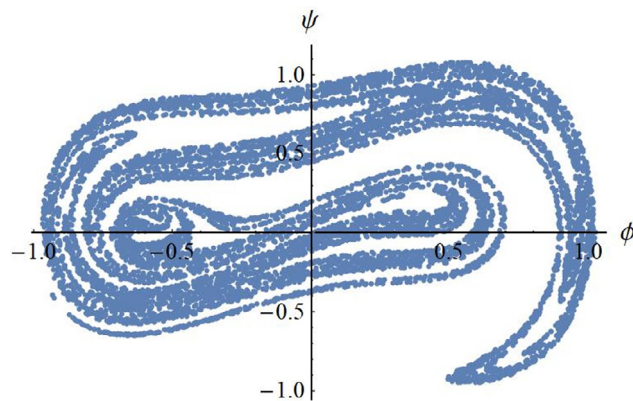
Fig. 8. Poincaré map of the system for parameter values associated with Fig. 6.
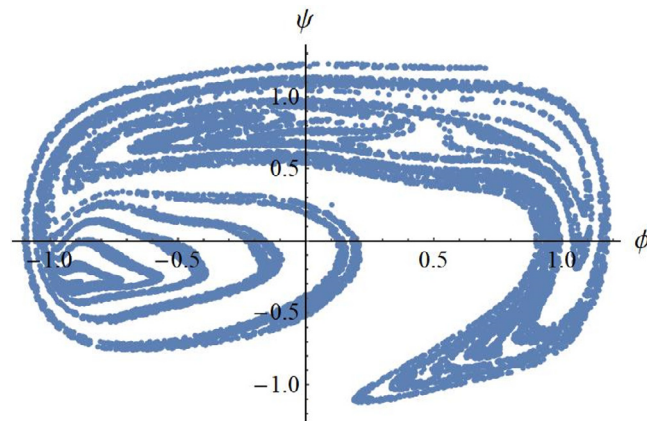
Fig. 9. Poincaré map of the system for parameter values associated with Fig. 7.

The only approximation used in the study of chaotic dynamics of nano-sensor includes employing the corresponding homoclinic and heteroclinic orbits of the Duffing equation instead of orbits of the original system. In previous research [57,59,63,64,70–72], a Taylor's third-order expansion of electrostatic force was used to investigate the Melnikov chaos of micro- and nano-systems based on the orbits of the Duffing equation. In this study, Taylor's fifth-order expansion of electrostatic force along with the corresponding orbits of the Duffing equation was employed to investigate Melnikov chaos, and the existence of non-zero coefficients c4 and c5 in the Melnikov criteria Eqs. (38) and ((40)) indicates a more accurate prediction of chaos than previous studies.

In view of Eqs. (B1) and B2) in Appendix A, it is observed that the obtained Melnikov criteria (Eqs. (38) and ((40)) in addition to geometric and material properties depend on length scale parameters of nonlocal strain gradient elasticity theory. The dependence of the Melnikov criteria to length scale parameters demonstrates that employing the nonlocal strain gradient elasticity theory is of crucial importance for precise chaos prediction in a graphene-based mass sensor. It is also realized from Eqs. (B1) and (B2) that the parameters of the Melnikov criteria are functions of the position and amount of the nanoparticle which is attached to the graphene sheet and can influence the chaotic behavior of the graphene-based mass sensor.

As proved earlier, this system is prone to the occurrence of homoclinic and heteroclinic chaos. Eqs. (38) and (40) are two Melnikov criteria for predicting the chaotic nature of the system. These criteria must be taken into consideration during the design process to keep the system away from chaotic behavior. The Melnikov criteria obtained for mass nano-sensor are the necessary but not sufficient conditions, i.e. changing the amount of a single parameter may not provide a chaotic behavior. Therefore, it is not that simple to achieve the range of change for each parameter that causes chaotic dynamics. The Melnikov criteria Eqs. (38) and ((40)) implicitly include all material and geometrical parameters of the mass nano-sensor. The designer can simply change the allowable parameters to transmit the system to a safe region and suppressing the chaos.

7. Concluding remarks

This paper dealt with the study of nonlinear and chaotic dynamics of graphene-based mass sensor which consisted of an electrostatically actuated fully clamped graphene resonator with a concentrated attached mass. The equations of motion were derived employing the nonlocal strain gradient elasticity theory and reduced to an ordinary differential equation by means of the Galerkin decomposition method. The potential energy of the system was analyzed to investigate the possibility of occurrence of homoclinic and heteroclinic bifurcations. The Melnikov's integral method was employed to derive two necessary inequality equations as analytical criteria which indicated the susceptible region of the system for chaotic behavior. Due to the presence of length scale parameters of nonlocal strain gradient theory of elasticity in the Melnikov criteria, it was concluded that the classical theory of elasticity was not able to predict precisely the chaotic behavior of nano-resonators. It was also found that the position and amount of the attached mass can affect the chaotic behavior of the system. The chaotic regimes of the system were also studied through plotting the Lyapunov exponent diagrams, phase plane trajectories and Poincaré maps which verified the intrinsic chaotic nature of graphene-based mass sensors.

Appendix A

The governing equation of motion of the nano-resonater and the attached mass can be derived employing the extended Hamilton's principle in Eq. (13). Based on the nonlocal strain gradient theory, the virtual strain energy can be written as

$$\delta\Pi_U = \int_V (\sigma_{xx}\delta\varepsilon_{xx} + 2\sigma_{xy}\delta\varepsilon_{xy} + \sigma_{yy}\delta\varepsilon_{yy} + \sigma_{xx}^{(1)}\nabla\delta\varepsilon_{xx} + 2\sigma_{xy}^{(1)}\nabla\delta\varepsilon_{xy} + \sigma_{yy}^{(1)}\nabla\delta\varepsilon_{yy})dV$$

$$= \int_V \left[(\sigma_{xx} - \nabla\sigma_{xx}^{(1)})\delta\varepsilon_{xx} + 2(\sigma_{xy} - \nabla\sigma_{xy}^{(1)})\delta\varepsilon_{xy} + (\sigma_{yy} - \nabla\sigma_{yy}^{(1)})\delta\varepsilon_{yy} \right] dV$$

$$+ \left[\int_0^{L_y} \left(\int_{-h/2}^{h/2} \sigma_{xx}^{(1)}\delta\varepsilon_{xx}dz + 2\int_{-h/2}^{h/2} \sigma_{xy}^{(1)}\delta\varepsilon_{xy}dz + \int_{-h/2}^{h/2} \sigma_{yy}^{(1)}\delta\varepsilon_{yy}dz \right)dy \right]_0^{L_x}$$

$$+ \left[\int_0^{L_x} \left(\int_{-h/2}^{h/2} \sigma_{xx}^{(1)}\delta\varepsilon_{xx}dz + 2\int_{-h/2}^{h/2} \sigma_{xy}^{(1)}\delta\varepsilon_{xy}dz + \int_{-h/2}^{h/2} \sigma_{yy}^{(1)}\delta\varepsilon_{yy}dz \right)dx \right]_0^{L_y} \tag{A1}$$

Herein the stress resultants are introduced as

$$\begin{Bmatrix} N_{xx}, M_{xx} \\ N_{yy}, M_{yy} \\ N_{xy}, M_{xy} \end{Bmatrix} = \int_{-h/2}^{h/2} \begin{Bmatrix} t_{xx} \\ t_{yy} \\ t_{xt} \end{Bmatrix} (1, z)dz \tag{A2}$$

$$\begin{Bmatrix} N_{xx}^{(1)}, M_{xx}^{(1)} \\ N_{yy}^{(1)}, M_{yy}^{(1)} \\ N_{xy}^{(1)}, M_{xy}^{(1)} \end{Bmatrix} = \int_{-h/2}^{h/2} \begin{Bmatrix} \sigma_{xx}^{(1)} \\ \sigma_{yy}^{(1)} \\ \sigma_{xy}^{(1)} \end{Bmatrix} (1, z)dz \tag{A3}$$

By substituting Eq. (12) into Eq. (A1), in view of Eqs. (A2) and (A3), one can obtain the following expressions for the virtual strain energy in terms of displacements and stress resultants

$$\delta\Pi_U = \int_A \left[N_{xx}\frac{\partial w}{\partial x}\frac{\partial \delta w}{\partial x} - M_{xx}\frac{\partial^2 \delta w}{\partial x^2} + N_{xy}\left(\frac{\partial w}{\partial y}\frac{\partial \delta w}{\partial x} + \frac{\partial w}{\partial x}\frac{\partial \delta w}{\partial y} \right) \right.$$

$$\left. - 2M_{xy}\frac{\partial^2 \delta w}{\partial x \partial y} + N_{yy}\frac{\partial w}{\partial y}\frac{\partial \delta w}{\partial y} - M_{yy}\frac{\partial^2 \delta w}{\partial y^2} \right] dA$$

$$+ \left[\int_0^{L_y} \left(N_{xx}^{(1)}\frac{\partial w}{\partial x}\frac{\partial \delta w}{\partial x} - M_{xx}^{(1)}\frac{\partial^2 \delta w}{\partial x^2} + N_{xy}^{(1)}\left(\frac{\partial w}{\partial y}\frac{\partial \delta w}{\partial x} + \frac{\partial w}{\partial x}\frac{\partial \delta w}{\partial y} \right) \right. \right.$$

$$\left. \left. - 2M_{xy}^{(1)}\frac{\partial^2 \delta w}{\partial x \partial y} + N_{yy}^{(1)}\frac{\partial w}{\partial y}\frac{\partial \delta w}{\partial y} - M_{yy}^{(1)}\frac{\partial^2 \delta w}{\partial y^2} \right)dy \right]_0^{L_x}$$

$$+ \left[\int_0^{L_x} \left(N_{xx}^{(1)}\frac{\partial w}{\partial x}\frac{\partial \delta w}{\partial x} - M_{xx}^{(1)}\frac{\partial^2 \delta w}{\partial x^2} + N_{xy}^{(1)}\left(\frac{\partial w}{\partial y}\frac{\partial \delta w}{\partial x} + \frac{\partial w}{\partial x}\frac{\partial \delta w}{\partial y} \right) \right. \right.$$

$$\left. \left. - 2M_{xy}^{(1)}\frac{\partial^2 \delta w}{\partial x \partial y} + N_{yy}^{(1)}\frac{\partial w}{\partial y}\frac{\partial \delta w}{\partial y} - M_{yy}^{(1)}\frac{\partial^2 \delta w}{\partial y^2} \right)dx \right]_0^{L_y} \tag{A4}$$

The total kinetic energy of the mass nano-sensor (K) is the summation of the kinetic energy of the graphene sheet (K_G) and the kinetic energy of the attached mass (K_0). Neglecting rotary inertia of the nano-plate and considering only transverse deflection, the variation of the kinetic energy of the nano-plate can be written as

$$\delta K_G = \int_A \rho h \frac{\partial w}{\partial t}\delta\frac{\partial w}{\partial t}dA \tag{A5}$$

The kinetic energy of the concentrated attached mass is defined employing the Dirac delta function. The following main property of Dirac delta function

$$\int_{-\infty}^{+\infty} \delta_D(x^*)dx^* = 1 \tag{A6}$$

implies that the product $\delta_D(x^*)dx^*$ must be dimensionless and consequently the dimension of the Dirac delta function becomes the inverse (reciprocal) of its argument. Hence, the variation of the kinetic energy of the attached mass which is located at (x_0, y_0) can be stated as

$$\delta K_0 = \int_A m_0\delta_D(x - x_0)\delta_D(y - y_0)\frac{\partial w}{\partial t}\delta\frac{\partial w}{\partial t}dA \tag{A7}$$

By summing Eqs. (A5) and (A7), the variation of the kinetic energy of the mass sensor can be obtained as

$$\delta K = \int_A [\rho h + m_0\delta_D(x - x_0)\delta_D(y - y_0)]\frac{\partial w}{\partial t}\delta\frac{\partial w}{\partial t}dA \tag{A8}$$

also, the virtual work due to electrostatic and damping forces is as follows:

$$\delta W_E = \int_A \left(F_E - C_D\frac{\partial w}{\partial t} \right)\delta w dA \tag{A9}$$

where C_D is the coefficient of the viscous damping coefficient per unit area and F_E is the electrostatic force per unit area of the graphene sheet.

The electrostatic force per unit area of the graphene sheet can be expressed as [73–76]

$$F_E = \frac{\varepsilon_0(V_{DC} + V_{AC}\sin\omega t)^2}{2(g-w)^2} \tag{A10}$$

where ε_0 is the permittivity of the gap medium and V_{DC} and V_{AC} are the bias DC voltage and harmonic excitation voltage, respectively, and g is the initial gap distance between the graphene and the ground plate.

Substituting Eqs. (A4), (A8) and (A9) into Eq. (13), applying integration by parts and doing some mathematical process lead to the equation of motion and corresponding classical and non-classical boundary conditions of the system as follows: equation of motion:

$$\frac{\partial}{\partial x}\left(N_{xx}\frac{\partial w}{\partial x} + N_{xy}\frac{\partial w}{\partial y}\right) + \frac{\partial}{\partial y}\left(N_{xy}\frac{\partial w}{\partial x} + N_{yy}\frac{\partial w}{\partial y}\right)$$

$$+ \frac{\partial^2 M_{xx}}{\partial x^2} + 2\frac{\partial^2 M_{xy}}{\partial x\partial y} + \frac{\partial^2 M_{yy}}{\partial y^2} + \left(F_E - C_D\frac{\partial w}{\partial t}\right)$$

$$= [\rho h + m_0\delta_D(x-x_0)\delta_D(y-y_0)]\frac{\partial^2 w}{\partial t^2} \tag{A11}$$

classical boundary conditions: at $x = 0$ or L_x

$$\text{either } \delta w = 0 \text{ or } N_{xx}\frac{\partial w}{\partial x} + N_{xy}\frac{\partial w}{\partial y} + \frac{\partial M_{xx}}{\partial x} + \frac{\partial M_{xy}}{\partial y} = 0$$

$$\text{either } \frac{\partial w}{\partial x} = 0 \text{ or } M_{xx} = 0$$

$$\text{either } \frac{\partial w}{\partial y} = 0 \text{ or } M_{xy} = 0 \tag{A12}$$

at $y = 0$ or L_y

$$\text{either } \delta w = 0 \text{ or } N_{xy}\frac{\partial w}{\partial x} + N_{yy}\frac{\partial w}{\partial y} + \frac{\partial M_{xy}}{\partial x} + \frac{\partial M_{yy}}{\partial y} = 0$$

$$\text{either } \frac{\partial w}{\partial x} = 0 \text{ or } M_{xy} = 0$$

$$\text{either } \frac{\partial w}{\partial y} = 0 \text{ or } M_{yy} = 0 \tag{A13}$$

non-classical boundary conditions: at $x = 0$ or L_x and $y = 0$ or L_y

$$\text{either } \frac{\partial w}{\partial x} = 0 \text{ or } N_{xx}^{(1)}\frac{\partial w}{\partial x} = 0$$

$$\text{either } \frac{\partial^2 w}{\partial x^2} = 0 \text{ or } M_{xx}^{(1)} = 0$$

$$\text{either } \frac{\partial w}{\partial x}\frac{\partial w}{\partial y} = 0 \text{ or } N_{xy}^{(1)} = 0$$

$$\text{either } \frac{\partial^2 w}{\partial x\partial y} = 0 \text{ or } M_{xy}^{(1)} = 0$$

$$\text{either } \frac{\partial w}{\partial y} = 0 \text{ or } N_{yy}^{(1)}\frac{\partial w}{\partial y} = 0$$

$$\text{either } \frac{\partial^2 w}{\partial y^2} = 0 \text{ or } M_{yy}^{(1)} = 0 \tag{A14}$$

Integrating Eq. (9) along the z-axis of the nano-plate yields

$$(1 - \mu\nabla^2)\begin{Bmatrix}N_{xx}\\N_{yy}\\N_{xy}\end{Bmatrix} = (1 - \lambda\nabla^2)\begin{bmatrix}A_{11} & A_{12} & 0\\A_{12} & A_{22} & 0\\0 & 0 & A_{66}\end{bmatrix}\begin{Bmatrix}(\partial w/\partial x)^2\\(\partial w/\partial y)^2\\(\partial w/\partial x)(\partial w/\partial y)\end{Bmatrix} \tag{A15}$$

Also, multiplying both sides of Eq. (9) to z then integrating over the thickness leads to:

$$(1 - \mu\nabla^2)\begin{Bmatrix}M_{xx}\\M_{yy}\\M_{xy}\end{Bmatrix} = (1 - \lambda\nabla^2)\begin{bmatrix}B_{11} & B_{12} & 0\\B_{12} & B_{22} & 0\\0 & 0 & B_{66}\end{bmatrix}\begin{Bmatrix}\partial^2 w/\partial x^2\\\partial^2 w/\partial y^2\\\partial^2 w/\partial x\partial y\end{Bmatrix} \tag{A16}$$

where A_{ij} and B_{ij} are as follows:

$$\begin{Bmatrix} A_{11}, B_{11} \\ A_{22}, B_{22} \\ A_{12}, B_{12} \\ A_{66}, B_{66} \end{Bmatrix} = \left(\frac{h}{2}, \frac{-h^3}{12} \right) \begin{Bmatrix} Q_{11} \\ Q_{22} \\ Q_{12} \\ Q_{66} \end{Bmatrix} \tag{A17}$$

In order to obtain the equation of motion in terms of the transverse displacement, stress resultants must be eliminated from Eq. (A11). Since, in this study, the mid-plane displacements are considered to be zero ($u_{x0}=u_{y0}=0$) and no force is applied to the plate in the x and y directions, the in-plane forces can be assumed to be constant. Based on this assumption, Reddy [77] adopted that the first two terms of Eq. (A11) can be linearized as follows to overcome this great challenge:

$$\frac{\partial}{\partial x}\left(N_{xx}\frac{\partial w}{\partial x} + N_{xy}\frac{\partial w}{\partial y} \right) + \frac{\partial}{\partial y}\left(N_{xy}\frac{\partial w}{\partial x} + N_{yy}\frac{\partial w}{\partial y} \right)$$

$$\approx N_{xx}\frac{\partial^2 w}{\partial x^2} + 2N_{xy}\frac{\partial^2 w}{\partial x \partial y} + N_{yy}\frac{\partial^2 w}{\partial y^2} \tag{A18}$$

Finally, an explicit expression is derived for the governing equation of motion directly in terms of the displacement by using Eq. (A18) in Eq. (A11) and in view of Eqs. (A15) and (A16).

Appendix B

The coefficients appearing in Eq. (23) are defined as

$$\alpha = \frac{-3}{4\eta}Eh^3\bar{C}_D\left(3L_xL_y + 4\pi^2\bar{\mu}^2(L_x^2 + L_y^2)\right)$$

$$\beta_0 = \frac{1}{\eta}Eh^3\bar{\varepsilon}L_xL_y$$

$$\beta_1 = \frac{1}{\eta}\Big[8B_{66} + \frac{12B_{11}L_y^3\pi^4}{L_x} + \frac{9}{2}Eh^3L_xL_y\bar{\varepsilon} + 32B_{66}(L_x^2 + L_y^2)\pi^6\bar{\lambda}^2$$

$$+ 16B_{11}L_y^2\pi^6\bar{\lambda}^2 + \frac{48B_{11}L_y^4\pi^6\bar{\lambda}^2}{L_x^2} + \frac{4B_{22}L_x^2\pi^4(3L_xL_y + 12L_x^2\pi^2\bar{\lambda}^2 + 4L_y^2\pi^2\bar{\lambda}^2)}{L_y^2}$$

$$+ 8B_{12}\left(L_xL_y\pi^4 + 4(L_x^2 + L_y^2)\pi^6\bar{\lambda}^2\right) + 6Eh^3(L_x^2 + L_y^2)\pi^2\bar{\varepsilon}\,\bar{\mu}^2\Big]$$

$$\beta_2 = \frac{15}{4\eta}Eh^3\bar{\epsilon}\left(5L_xL_y + 8(L_x^2 + L_y^2)\pi^2\bar{\mu}^2\right)$$

$$\beta_3 = \frac{5}{16\eta L_x^2}\Big[-120A_{12}g^2L_x^3L_y\pi^4 - 28A_{11}g^2L_xL_y^3\pi^4 + 245Eh^3L_x^3L_y\bar{\varepsilon}$$

$$-64A_{11}g^2L_x^2L_y^2\pi^6\bar{\lambda}^2 + 448A_{11}g^2L_y^4\pi^6\bar{\lambda}^2 + 420Eh^3L_x^4\pi^2\bar{\varepsilon}\bar{\mu}^2$$

$$+ \frac{4A_{22}g^2L_x^4\pi^4}{L_y^2}\left(-7L_xL_y + 112(L_x^2 + L_y^2)\pi^2\bar{\lambda}^2\right) + 420Eh^3L_x^2L_y^2\pi^2\bar{\varepsilon}\bar{\mu}^2$$

$$+ 8A_{66}g^2L_x^2\pi^2\left(5L_xL_y + 32(L_x^2 + L_y^2)\pi^2\bar{\lambda}^2\right)\Big]$$

$$\beta_4 = \frac{2205}{64\eta}Eh^3\bar{\epsilon}\left(9L_xL_y + 16(L_x^2 + L_y^2)\pi^2\bar{\mu}^2\right)$$

$$\beta_5 = \frac{14553}{128\eta}Eh^3\bar{\epsilon}\left(11L_xL_y + 20(L_x^2 + L_y^2)\pi^2\bar{\mu}^2\right)$$

$$c_0 = -\frac{2}{\eta}Eh^3\bar{\epsilon}L_xL_y$$

$$c_1 = -\frac{3}{\eta}Eh^3\bar{\epsilon}\left(3L_xL_y + 4\pi^2\bar{\mu}^2(L_x^2 + L_y^2)\right)$$

$$c_2 = -\frac{7}{2\eta}Eh^3\bar{\epsilon}\left(5L_xL_y + 8\pi^2\bar{\mu}^2(L_x^2 + L_y^2)\right)$$

$$c_3 = -\frac{175}{8\eta}Eh^3\bar{\epsilon}\left(7L_xL_y + 12\pi^2\bar{\mu}^2(L_x^2 + L_y^2)\right)$$

$$c_4 = -\frac{2205}{32\eta}Eh^3\bar{\epsilon}\left(9L_xL_y + 16\pi^2\bar{\mu}^2(L_x^2 + L_y^2)\right)$$

$$c_5 = -\frac{14553}{64\eta}Eh^3\bar{\epsilon}\left(11L_xL_y + 20\pi^2\bar{\mu}^2(L_x^2 + L_y^2)\right) \tag{B1}$$

in which

$$
\begin{aligned}
\eta = \frac{1}{4}Eh^3 \Big\{ &-9L_xL_y - 12L_x^2\pi^2\bar{\mu}^2 - 12L_y^2\pi^2\bar{\mu}^2 + 32\bar{m}\Big[L_y\big(-L_x + 2L_y\pi^2\bar{\mu}^2\big) \\
&+ \big(L_xL_y + 4L_x^2\pi^2\bar{\mu}^2 - 2L_y^2\pi^2\bar{\mu}^2\big)\cos(2\pi y_0)\Big]\sin^4(\pi x_0)\sin^2(\pi y_0) \\
&- 512\bar{m}L_y^2\pi^2\bar{\mu}^2\cos^4(\pi x_0/2)\cos(\pi x_0)(-7 + 8\cos(\pi x_0))\sin^4(\pi y_0) \\
&+ 128\bar{m}L_y^2\pi^2\bar{\mu}^2\cos^2(\pi x_0/2)(5 - 10\cos(\pi x_0) + 9\cos(2\pi x_0))\sin^4(\pi y_0) \\
&- 160\bar{m}L_y^2\pi^2\bar{\mu}^2\sin^2(\pi x_0/2)\sin^4(\pi y_0) \Big\}
\end{aligned}
\tag{B2}
$$

References

[1] H.-Y. Chiu, P. Hung, H.W.C. Postma, M. Bockrath, Atomic-Scale mass sensing using carbon nanotube resonators, Nano Lett. 8 (2008) 4342–4346.
[2] B. Lassagne, D. Garcia-Sanchez, A. Aguasca, A. Bachtold, Ultrasensitive mass sensing with a nanotube electromechanical resonator, Nano Lett. 8 (2008) 3735–3738.
[3] J. Chaste, A. Eichler, J. Moser, G. Ceballos, R. Rurali, A. Bachtold, A nanomechanical mass sensor with yoctogram resolution, Nat. Nanotechnol. 7 (2012) 301.
[4] K.S. Novoselov, A.K. Geim, S.V. Morozov, D. Jiang, Y. Zhang, S.V. Dubonos, I.V. Grigorieva, A.A. Firsov, Electric field effect in atomically thin carbon films, Science 306 (2004) 666.
[5] K.S. Novoselov, V.I. Fal'ko, L. Colombo, P.R. Gellert, M.G. Schwab, K. Kim, A roadmap for graphene, Nature 490 (2012) 192.
[6] X.-W. Lei, T. Natsuki, J.-X. Shi, Q.-Q. Ni, An atomic-resolution nanomechanical mass sensor based on circular monolayer graphene sheet: theoretical analysis of vibrational properties, J. Appl. Phys 113 (2013) 154313.
[7] A. Sakhaee-Pour, M.T. Ahmadian, A. Vafai, Applications of single-layered graphene sheets as mass sensors and atomistic dust detectors, Solid State Commun. 145 (2008) 168–172.
[8] C. Li, T.-W. Chou, Single-walled carbon nanotubes as ultrahigh frequency nanomechanical resonators, Phys. Rev. B 68 (2003) 073405.
[9] C. Chen, S. Rosenblatt, K.I. Bolotin, W. Kalb, P. Kim, I. Kymissis, H.L. Stormer, T.F. Heinz, J. Hone, Performance of monolayer graphene nanomechanical resonators with electrical readout, Nat. Nano 4 (2009) 861–867.
[10] M. Sadeghi, R. Naghdabadi, Nonlinear vibrational analysis of single-layer graphene sheets, Nanotechnology 21 (2010) 105705.
[11] J.R. Mianroodi, S.A. Niaki, R. Naghdabadi, M. Asghari, Nonlinear membrane model for large amplitude vibration of single layer graphene sheets, Nanotechnology 22 (2011) 305703.
[12] H.M. Ouakad, M.I. Younis, Natural frequencies and mode shapes of initially curved carbon nanotube resonators under electric excitation, J. Sound Vib. 330 (2011) 3182–3195.
[13] J.W. Kang, H.-W. Kim, K.-S. Kim, J.H. Lee, Molecular dynamics modeling and simulation of a graphene-based nanoelectromechanical resonator, Curr. Appl. Phy. 13 (2013) 789–794.
[14] A.M. Eriksson, D. Midtvedt, A. Croy, A. Isacsson, Frequency tuning, nonlinearities and mode coupling in circular mechanical graphene resonators, Nanotechnology 24 (2013) 395702.
[15] H. Lee, J.-C. Hsu, S.-Y. Lin, W.-J. Chang, Sensitivity analysis of single-layer graphene resonators using atomic finite element method, J. Appl. Phys. 114 (2013) 123506-123506.
[16] D.I. Caruntu, L. Luo, Frequency response of primary resonance of electrostatically actuated CNT cantilevers, Nonlinear Dyn. 78 (2014) 1827–1837.
[17] S. Jiang, X. Gong, X. Guo, X. Wang, Potential application of graphene nanomechanical resonator as pressure sensor, Solid State Commun. 193 (2014) 30–33.
[18] P. Weber, J. Güttinger, A. Noury, J. Vergara-Cruz, A. Bachtold, Force sensitivity of multilayer graphene optomechanical devices, Nat. Commun. 7 (2016) 12496.
[19] J.W. Kang, H.J. Hwang, K.-S. Kim, Molecular dynamics study on vibrational properties of graphene nanoribbon resonator under tensile loading, Comput. Mater. Sci. 65 (2012) 216–220.
[20] H.-S. Shen, Y.-M. Xu, C.-L. Zhang, Prediction of nonlinear vibration of bilayer graphene sheets in thermal environments via molecular dynamics simulations and nonlocal elasticity, Comput. Methods Appl. Mech. Eng. 267 (2013) 458–470.
[21] M.A. Eltaher, N. Mohamed, S. Mohamed, L.F. Seddek, Postbuckling of curved carbon nanotubes using energy equivalent model, J. Nano Res. 57 (2019) 136–157.
[22] Y. Wu, X. Zhang, A.Y.T. Leung, W. Zhong, An energy-equivalent model on studying the mechanical properties of single-walled carbon nanotubes, Thin-Walled Struct. 44 (2006) 667–676.
[23] M.A. Eltaher, M. Agwa, A. Kabeel, Vibration analysis of material size-dependent CNTs using energy equivalent model, J. Appl. Comput. Mech. 4 (2018) 75–86.
[24] L. Shen, H.-S. Shen, C.-L. Zhang, Nonlocal plate model for nonlinear vibration of single layer graphene sheets in thermal environments, Comput. Mater. Sci. 48 (2010) 680–685.
[25] R. Ansari, S. Sahmani, B. Arash, Nonlocal plate model for free vibrations of single-layered graphene sheets, Phys. Lett. A 375 (2010) 53–62.
[26] L.W. Zhang, Y. Zhang, K.M. Liew, Modeling of nonlinear vibration of graphene sheets using a meshfree method based on nonlocal elasticity theory, Appl. Math. Model. 49 (2017) 691–704.
[27] M.S. Nematollahi, H. Mohammadi, M.A. Nematollahi, Thermal vibration analysis of nanoplates based on the higher-order nonlocal strain gradient theory by an analytical approach, Superlattices Microstruct. 111 (2017) 944–959.
[28] F. Ebrahimi, M.R. Barati, Damping vibration analysis of graphene sheets on viscoelastic medium incorporating hygro-thermal effects employing nonlocal strain gradient theory, Compos. Struct. 185 (2018) 241–253.
[29] F. Ebrahimi, M.R. Barati, Vibration analysis of nonlocal strain gradient embedded single-layer graphene sheets under nonuniform in-plane loads, J. Vib. Control 24 (2017) 4751–4763.
[30] S. Sahmani, M.M. Aghdam, T. Rabczuk, Nonlocal strain gradient plate model for nonlinear large-amplitude vibrations of functionally graded porous micro/nano-plates reinforced with GPLs, Compos. Struct. 198 (2018) 51–62.
[31] D. Shahsavari, B. Karami, L. Li, Damped vibration of a graphene sheet using a higher-order nonlocal strain-gradient Kirchhoff plate model, Comptes Rendus Mécanique 346 (2018) 1216–1232.
[32] B. Arash, Q. Wang, W.H. Duan, Detection of gas atoms via vibration of graphenes, Phys. Lett. A 375 (2011) 2411–2415.
[33] J.W. Jiang, H.S. Park, T. Rabczuk, Enhancing the mass sensitivity of graphene nanoresonators via nonlinear oscillations: the effective strain mechanism, Nanotechnology 23 (2012) 475501.
[34] M.D. Dai, C.-W. Kim, K. Eom, Nonlinear vibration behavior of graphene resonators and their applications in sensitive mass detection, Nanoscale Res. Lett. 7 (2012) 499.
[35] Z.-B. Shen, H.-L. Tang, D.-K. Li, G.-J. Tang, Vibration of single-layered graphene sheet-based nanomechanical sensor via nonlocal Kirchhoff plate theory, Comput. Mater. Sci. 61 (2012) 200–205.
[36] H.-L. Lee, Y.-C. Yang, W.-J. Chang, Mass detection using a graphene-based nanomechanical resonator, Jpn. J. Appl. Phys. 52 (2013) 025101.

[37] O.K. Kwon, K.-S. Kim, J. Park, J.W. Kang, Molecular dynamics modeling and simulations of graphene-nanoribbon-resonator-based nanobalance as yoc-togram resolution detector, Comput. Mater. Sci. 67 (2013) 329–333.
[38] T. Murmu, S. Adhikari, Nonlocal mass nanosensors based on vibrating monolayer graphene sheets, Sens. Actuat. B 188 (2013) 1319–1327.
[39] Q. Wang, B. Arash, A review on applications of carbon nanotubes and graphenes as nano-resonator sensors, Comput. Mater. Sci. 82 (2014) 350–360.
[40] S.A. Fazelzadeh, E. Ghavanloo, Nanoscale mass sensing based on vibration of single-layered graphene sheet in thermal environments, Acta Mechanica Sinica 30 (2014) 84–91.
[41] S.-M. Zhou, L.-P. Sheng, Z.-B. Shen, Transverse vibration of circular graphene sheet-based mass sensor via nonlocal Kirchhoff plate theory, Comput. Mater. Sci. 86 (2014) 73–78.
[42] S.K. Jalali, M.H. Naei, N.M. Pugno, Graphene-Based resonant sensors for detection of ultra-fine nanoparticles: molecular dynamics and nonlocal elas-ticity investigations, Nano 10 (2015) 1550024.
[43] D. Karličić, P. Kozić, S. Adhikari, M. Cajić, T. Murmu, M. Lazarević, Nonlocal mass-nanosensor model based on the damped vibration of single-layer graphene sheet influenced by in-plane magnetic field, Int. J. Mech. Sci. 96–97 (2015) 132–142.
[44] R.W. Jiang, Z.B. Shen, G.J. Tang, Vibration analysis of a single-layered graphene sheet-based mass sensor using the Galerkin strip distributed transfer function method, Acta Mech. 227 (2016) 2899–2910.
[45] M.A. Eltaher, M.A. Agwa, Analysis of size-dependent mechanical properties of CNTs mass sensor using energy equivalent model, Sens. Actuat. A 246 (2016) 9–17.
[46] F. Ebrahimi, M.R. Barati, A nonlocal strain gradient mass sensor based on vibrating hygro-thermally affected graphene nanosheets, Iran. J. Sci. Technol. Trans. Mech. Eng. (2017).
[47] B.E. DeMartini, H.E. Butterfield, J. Moehlis, K.L. Turner, Chaos for a microelectromechanical oscillator governed by the nonlinear mathieu equation, J. Microelectromech. Syst. 16 (2007) 1314–1323.
[48] A.Y. Joshi, S.C. Sharma, S.P. Harsha, Nonlinear dynamic analysis of single-walled carbon nanotube based mass sensor, J. Nanotechnol. Eng. Med. 2 (2012) 041008-041008-041006.
[49] A.Y. Joshi, S.C. Sharma, S.P. Harsha, Chaotic response analysis of single-walled carbon nanotube due to surface deviations, Nano 7 (2012) 1250008.
[50] L. Jin, X. Wang, L. Li, Chaotic synchronization of two microresonators with application in mass sensors, J. Appl. Phys. 113 (2013) 093506.
[51] A.C. Eringen, Nonlocal polar elastic continua, Int. J. Eng. Sci. 10 (1972) 1–16.
[52] A.C. Eringen, On differential equations of nonlocal elasticity and solutions of screw dislocation and surface waves, J. Appl. Phys. 54 (1983) 4703–4710.
[53] D.C. Lam, F. Yang, A. Chong, J. Wang, P. Tong, Experiments and theory in strain gradient elasticity, J. Mech. Phys. Solid. 51 (2003) 1477–1508.
[54] C. Lim, G. Zhang, J. Reddy, A higher-order nonlocal elasticity and strain gradient theory and its applications in wave propagation, J. Mech. Phys. Solid. 78 (2015) 298–313.
[55] E.C. Aifantis, On the role of gradients in the localization of deformation and fracture, Int. J. Eng. Sci. 30 (1992) 1279–1299.
[56] H.S. Haghighi, A.H.D. Markazi, Chaos prediction and control in MEMS resonators, Commun. Nonlinear Sci. Numer. Simul. 15 (2010) 3091–3099.
[57] E. Maani Miandoab, H.N. Pishkenari, A. Yousefi-Koma, F. Tajaddodianfar, Chaos prediction in MEMS-NEMS resonators, Int. J. Eng. Sci. 82 (2014) 74–83.
[58] M.S. Siewe, U.H. Hegazy, Homoclinic bifurcation and chaos control in MEMS resonators, Appl. Math. Model. 35 (2011) 5533–5552.
[59] S. Zhankui, K. Sun, Nonlinear and chaos control of a micro-electro-mechanical system by using second-order fast terminal sliding mode control, Commun. Nonlinear Sci. Numer. Simul. 18 (2013) 2540–2548.
[60] M. Shokravi, Dynamic pull-in and pull-out analysis of viscoelastic nanoplates under electrostatic and Casimir forces via sinusoidal shear deformation theory, Microelectron. Reliab. 71 (2017) 17–28.
[61] A. Sakhaee-Pour, M.T. Ahmadian, R. Naghdabadi, Vibrational analysis of single-layered graphene sheets, Nanotechnology 19 (2008) 085702.
[62] A.W. Leissa, Vibration of Plates, Government Printing Office, Washington DC: US, 1969.
[63] E.M. Miandoab, A. Yousefi-Koma, H.N. Pishkenari, F. Tajaddodianfar, Study of nonlinear dynamics and chaos in MEMS/NEMS resonators, Commun. Nonlinear Sci. Num. Simul. 22 (2015) 611–622.
[64] F. Tajaddodianfar, H. Nejat Pishkenari, M.R. Hairi Yazdi, Prediction of chaos in electrostatically actuated arch micro-nano resonators: analytical ap-proach, Commun. Nonlinear Sci. Num. Simul. 30 (2016) 182–195.
[65] B.B. Ali, H. Nayfeh, Applied Nonlinear Dynamics: Analytical, Computational, and Experimental Methods, John Wiley & Sons, New York, 2007.
[66] P.H. John Guckenheimer, Nonlinear Oscillations, Dynamical Systems, and Bifurcations of Vector Fields, Springer, New York, 2002.
[67] S. Wiggins, Introduction to Applied Nonlinear Dynamical Systems and Chaos, Springer, New York, 2003.
[68] M. Siewe Siewe, C. Tchawoua, P. Woafo, Melnikov chaos in a periodically driven Rayleigh–Duffing oscillator, Mech. Res. Commun. 37 (2010) 363–368.
[69] F.C. Moon, Chaotic Vibrations: An Introduction For Applied Scientists and Engineers, John Wiley & Sons, New Jersey, 2005.
[70] H.S. Haghighi, A.H. Markazi, Chaos prediction and control in MEMS resonators, Commun. Nonlinear Sci. Num. Simul. 15 (2010) 3091–3099.
[71] M. Maleki, H. Nahvi, Nano-resonator dynamic behavior based on nonlocal elasticity theory, proceedings of the institution of mechanical engineers, Part C 229 (2015) 2665–2671.
[72] F. Tajaddodianfar, H. Nejat Pishkenari, M.R. Hairi Yazdi, E. Maani Miandoab, On the dynamics of bistable micro/nano resonators: analytical solution and nonlinear behavior, Commun. Nonlinear Sci. Num. Simul. 20 (2015) 1078–1089.
[73] D.H.B. John, A. Pelesko, Modeling MEMS and NEMS, CRC Press, 2002.
[74] A. Nabian, G. Rezazadeh, M. Haddad-derafshi, A. Tahmasebi, Mechanical behavior of a circular micro plate subjected to uniform hydrostatic and non-uniform electrostatic pressure, Microsyst. Technol. 14 (2007) 235–240.
[75] K.F. Wang, B.L. Wang, S. Zeng, Small scale effect on the pull-in instability and vibration of graphene sheets, Microsyst. Technol. 23 (2016) 2033–2041.
[76] W.D. Yang, W.B. Kang, X. Wang, Thermal and surface effects on the pull-in characteristics of circular nanoplate NEMS actuator based on nonlocal elasticity theory, Appl. Math. Model. 43 (2017) 321–336.
[77] J.N. Reddy, Nonlocal nonlinear formulations for bending of classical and shear deformation theories of beams and plates, Int. J. Eng. Sci. 48 (2010) 1507–1518.